Doping and phonon renormalization in carbon nanotubes

J. C. TSANG[1], M. FREITAG[1], V. PEREBEINOS[1], J. LIU[2] AND PH. AVOURIS[1]*

[1]IBM, T. J. Watson Research Center, Yorktown Heights, New York 10598, USA
[2]Department of Chemistry, Duke University, North Carolina 27708, USA
*e-mail: avouris@us.ibm.com

Published online: 14 October 2007; doi:10.1038/nnano.2007.321

We show that the Raman frequency associated with the vibrational mode at $\sim$1,580 cm^{-1} (the G mode) in both metallic and semiconducting carbon nanotubes shifts in response to changes in the charge density induced by an external gate field. These changes in the Raman spectra provide us with a powerful tool for probing local doping in carbon nanotubes in electronic device structures, or charge carrier densities induced by environmental interactions, on a length scale determined by the light diffraction limit. The G mode shifts to higher frequency and narrows in linewidth in metallic carbon nanotubes at large fields. This behaviour is analogous to that observed recently in graphene. In semiconducting carbon nanotubes, on the other hand, induced changes in the charge density only shift the phonon frequency, but do not affect its linewidth. These spectral changes are quantitatively explained by a model that involves the renormalization of the carbon nanotube phonon energy by the electron–phonon interaction as the carrier density in the carbon nanotube is changed.

Any future electronic technology based on field-effect devices will require the fabrication of high-mobility channels that are much smaller than those in existing complementary metal oxide semiconductor (CMOS) devices[1]. Carbon nanotube (CNT) field-effect transistors (CNTFET) have outstanding electrical transport properties and provide ideal model systems to address the technical challenge of how to build and characterize nanoscale electronic devices[2–5]. However, because their single-atomic-layer structure is exposed, and electronic screening within the layer is weak, the electronic properties of carbon nanotubes are particularly susceptible to environmental interactions. These include charge transfer with adsorbed molecules[6–9], electrostatic doping by fields created, for example, by trapped charges in the insulating substrate or gate oxide[10–12], or even pH variations for dispersed nanotubes[13]. Such interactions are typically localized and result in charge density variations between different nanotubes in an integrated circuit, or along the channel of a single CNTFET. The successful implementation of nanotube-based electronics and an understanding of charge transfer interactions and doping will require the ability to directly measure the local charge density in a nanotube. We propose here an approach based on the correlation between the shift in the frequency of a Raman phonon peak and an induced change in charge density in a carbon nanotube.

In this paper, we specifically measure and model theoretically the changes in optical phonon frequencies and widths in both semiconducting and metallic CNTFETs in response to electrostatic doping induced by the application of a gate voltage V_g in a FET configuration. By varying V_g, we controllably and reversibly change the charge density and the Fermi level in the CNT. Moving away from the intrinsic state of the CNT leads to a blueshift of the G phonon frequency of the CNTs. The shifts we measure are comparable in magnitude to the V_g-induced phonon shifts reported recently for the G line in zero-gap, graphene devices[14,15]. Here, we focus on weak doping that does not distort the electronic structure, as in the case of nanotubes or graphite strongly intercalated with donors or acceptors[16].

We can account theoretically for the observed changes in Raman energy by the renormalization of the phonon energy by the electron–phonon interaction, the importance of which was recognized long ago[17,18]. Although no static distortions are expected at room temperature in CNTs, 'dynamical distortions' (that is, non-adiabatic corrections) can lead to a large polaronic renormalization of the bandgap of the order of 50–100 meV in semiconducting CNTs (ref. 19). The origin of the polaron binding, due to the coupling of electrons (or holes) with the 'phonon cloud', has been extensively discussed[20], and its scaling with the strength of the electron–phonon coupling $W_{\mathrm{e-ph}}$ as $W^2_{\mathrm{e-ph}}/\hbar\omega$, where $\hbar\omega$ is the phonon energy, can be understood in terms of second-order perturbation theory. At the same time, the electron–phonon interaction renormalizes $\hbar\omega$. This effect is typically an order of magnitude smaller, as from perturbation theory one expects a phonon energy scaling of $W^2_{\mathrm{e-ph}}/2\Delta$, where 2Δ is the energy of the effective gap. However, in metals with strong electron–optical phonon coupling strength, and in cases like graphene where the phonons have energies comparable to or larger than the gap, the dynamic effect can be especially large[21]. The energy renormalization in perturbation theory reduces the phonon energy, that is, has a negative sign, and has its maximum in undoped or intrinsic graphene and CNTs. Therefore, reducing the energy renormalization by applying a gate field can induce a blueshift in the Raman peak. A similar situation may be expected in the case of one-dimensional (1D) metallic nanotubes, although, as we show below, the effect becomes even stronger due to the reduced dimensionality of the system. Finally, and most importantly, we find that the renormalization of the phonon energy by carriers in semiconducting CNTs also results in a blueshift due, in this case, to the coupling of the Raman active phonons to virtual electron–hole pairs. Contrary to

© 2007 Nature Publishing Group

intuitive expectations, the shifts in semiconducting tubes can become even larger than in metallic tubes at the same doping level, especially for large-diameter tubes where the bandgap approaches the optical phonon energy. This is surprising, as closely related phenomena such as Kohn anomalies and charge density waves occur only in metallic systems[21–24]. We note that the interband electron–phonon coupling is responsible for the phonon renormalization, whereas the intraband electron–phonon coupling controls the Raman intensity.

In addition to the energy renormalization, the electron–phonon interaction gives rise to a finite lifetime of electrons and phonons. The former determines the transport properties of semiconducting carbon CNTs (refs 25–28), whereas the latter gives rise to the finite linewidth of the Raman phonon peaks, which has an additional contribution in metallic CNTs due to the phonon decay into electron–hole pair excitations[29]. In contrast, in the semiconductor, the phonon linewidth is dominated by anharmonic lattice effects as there are no real electronic transitions at the phonon energy. Our results suggest a novel optical method of measuring changes in the local doping in low-dimensional nanometre-scale systems, as the laser spot size used to excite Raman scattering is less than 500 nm in diameter in this work and could be smaller. As an optical method, it can also be applied to buried channels and its spatial resolution can be drastically increased using near-field excitation schemes.

In Fig. 1a, we show gate-voltage-dependent G-mode Raman spectra of a metallic nanotube incorporated in a FET structure. The width and shape of the G line under zero source–drain bias (V_{sd}) at $V_g = 0$ V is consistent with the Raman spectrum previously reported for metallic CNTs (ref. 30). There is a shift of about 10 cm^{-1} in the lower energy G^- component of the G phonon to higher frequencies as V_g is varied from 0 to −20 V for $V_{sd} = 0$ V. This frequency shift with V_g is fully reversible. Changes in the G-line Raman scattering from this metallic CNT for positive V_g are much smaller than the changes for negative V_g. This can be understood in terms of trapped electrons in the oxide, which screen part of the applied gate field under positive gate voltage and also lead to hysteresis in I–V_g sweeps. In addition to the frequency shifts, we also observe changes in the width of the dominant Raman line with changing V_g. For example, at $V_g = 0$ V, the full-width at half-maximum (FWHM) is 29.4 cm^{-1}, whereas at $V_g = -20$ V, it is 5.7 cm^{-1}. The Raman peak widths and shifts as a function of the gate bias, or induced linear charge density (in e nm^{-1}) are plotted in Fig. 1b,c along with the predictions (given by the solid lines) of the theoretical model that will be discussed in the next section. Both blue and red points were obtained from the same CNT device, but the red points were obtained after the device was exposed to air for a few days.

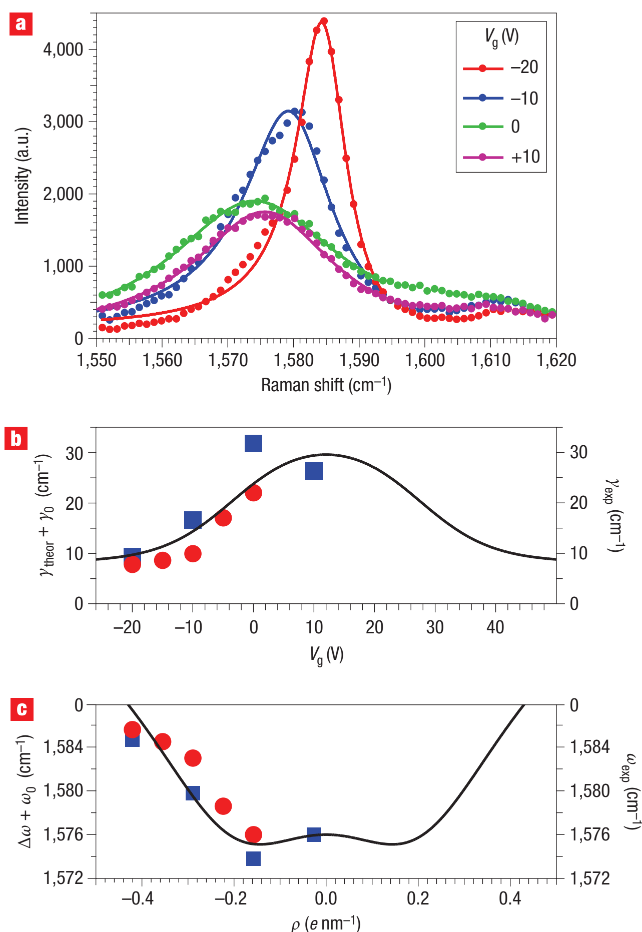

Figure 1 Raman spectra of a metallic CNT as a function of gate voltage. **a**, Spectra obtained under 514.5 nm excitation at different gate voltages along with Fano profile fits (solid curves). **b**,**c**, Theoretical width (**b**) and shift (**c**) versus charge density (black curves) for $d_{CNT} = 2.35$ nm, $D = 13$ eV Å^{-1}, $T = 450$ K and $\omega_0 = 1{,}576$ cm^{-1} compared with experiment (both blue and red points were obtained from the same CNT device, but the red points were obtained after the device was exposed to air for a few days). The x axis of **b** is centred about threshold gate voltage of $V_{th} = 12$ V for clarity. The theoretical width in **c** is broadened by $\gamma_0 = 8$ cm^{-1} to account for the anharmonic phonon decay and the finite experimental resolution.

In Fig. 2a, we show Raman spectra between 1,570 and 1,600 cm^{-1} from a semiconducting CNTFET for a range of V_g values between +18 V and −25 V. Over this range, our electrical measurements show that the device switched from the 'off' to the 'on' state with off currents of 0.1 nA, and on currents of about 1 μA for $V_{sd} = 0.1$ V. The Raman spectra were obtained with $V_{sd} = 0$ and gate leakage currents in the nA range. At $V_g = 0$ V, the spectrum in Fig. 2a is dominated by a lorentzian at 1,583 cm^{-1}, the higher energy G^+ mode of the CNT, with an intrinsic width of about 6 cm^{-1}. The asymmetry to lower energies in this spectrum can be assigned to a lorentzian at 1,573 cm^{-1}, a reasonable value for the G^- line in a sample with a diameter of about 2.4 nm. In Fig. 2a, the G-line Raman peak shows no shift for positive gate voltage, but shifts to higher energies by about 5 cm^{-1} as V_g becomes more negative. This dependence of the G^+ mode energy on V_g is reversible. In addition, the intensity of the G^+ line also shows reversible behaviour with changing V_g. It is independent of V_g for $V_g > 0$, and decreases with V_g as V_g become more negative, as seen in Fig. 2. Figure 2a also shows that there is no change in the width of this line with changing gate voltage. The V_g dependence of the G-line FWHM and energies for the spectra in Fig. 2a are shown in Fig. 2b and c, respectively, along with the theoretical predictions. The system spectral resolution is shown as the black line in Fig. 2b. Therefore, in contrast to the obvious change of the G^+ line energy with changing V_g, its width shows no quantitative change. Due to trapped charges in the gate oxide, the semiconducting device I–V characteristics also show strong hysteresis. For our scan range, the CNTFET turns on at our negative V_g, but has not turned on yet for our most positive V_g due to these negative trapped charges. Spatially resolved Raman results similar to the data in Fig. 2 show that the voltage-dependent shift of the G line to higher energies occurs uniformly along the device. Different devices show differences in the magnitude of the shift to higher energies with negative gate voltage.

© 2007 Nature Publishing Group

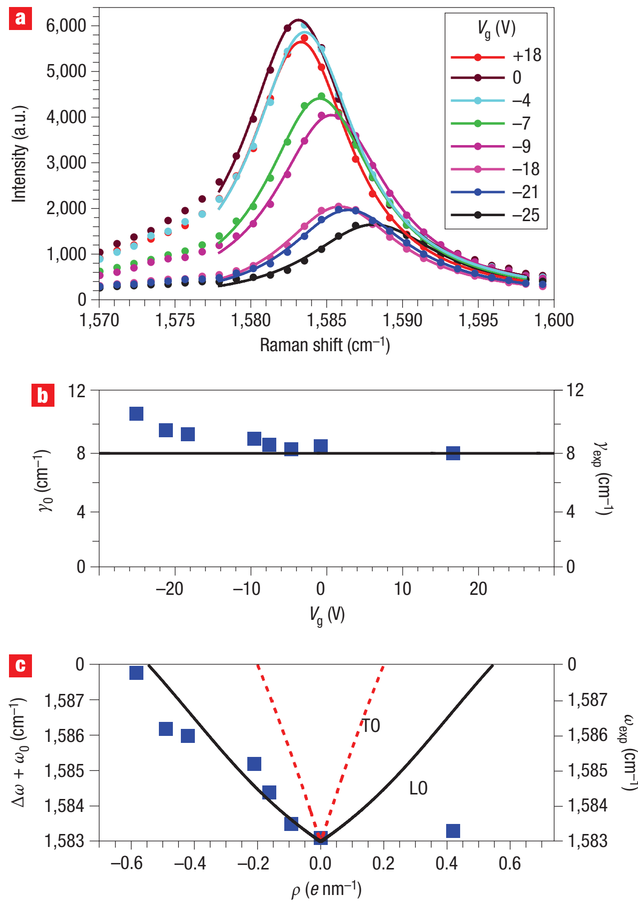

Figure 2 Raman spectra of a semiconducting CNT as a function of gate voltage. a, Raman spectra of a semiconducting CNTFET at several different values of V_g together with Fano profile fits (solid curves). **b**, Experimental width dependence on the gate voltage (blue squares) along with a constant width of $\gamma_0 = 8\ \mathrm{cm}^{-1}$ (black line) determined by the anharmonicity and instrumental resolution. **c**, Theoretical Raman shift for the LO mode (black curve) versus charge density obtained for $d = 2.35$ nm, $D = 13$ eV Å^{-1}, $T = 450$ K and $\omega_0 = 1{,}583\ \mathrm{cm}^{-1}$ compared with experiment (blue squares). The shift for the TO mode calculated with the same parameters is shown for comparison (red dotted curve). The x-axis is set by the threshold gate voltage of $V_{th} = 0$ V. V_g and ρ are linked by electrostatics through $\rho = C(V_g - V_{th})$.

To formally describe the induced shifts and broadening of the Raman spectra, we calculate the phonon self-energy to the lowest order in electron–phonon coupling, that is, within the Born approximation. The energy renormalization and the lifetime of a phonon with momentum q are given by the real and imaginary parts of the self-energy[31,32]:

$$\Delta\hbar\omega_q = \sum_k |W_{kq}|^2 \frac{\delta f_k - \delta f_{k+q}}{\varepsilon_k - \varepsilon_{k+q} + \hbar\omega_q} \qquad (1)$$

$$\gamma_q = \pi \sum_k |W_{kq}|^2 \delta(\varepsilon_k - \varepsilon_{k+q} + \hbar\omega_q)(f_k - f_{k+q}) \qquad (2)$$

where W_{kq} is the strength of the electron–phonon interaction and f_k is the electron distribution function, which is described by the Fermi–Dirac distribution with a variable chemical potential ε_F (refs 33–36). In equation (1), we consider changes in the distribution function $\delta f_k = f_k(\varepsilon_F) - f_k(\varepsilon_F = 0)$, that is, changes in ε_F induced by the environment or the gate potential, as we are interested in V_g-induced changes of the phonon renormalization energies. In the lowest order, renormalization energies are always negative (redshifted phonon energies); hence, we expect the gate-bias-induced changes to be positive (blueshifted phonon frequencies) for the simple band structures of graphene and CNTs. Specifically, we are interested in the Raman active phonon modes with zero momentum, $q = 0$. Only interband transitions can contribute to the phonon self-energy, otherwise $f_k - f_{k+q}$ is identically zero. Typically, a longitudinal optical phonon mode (LO) has the strongest Raman intensity in CNTs (refs 37, 38), but both LO and transverse (TO) degenerate optical phonons are simultaneously excited in Raman processes in graphene. To calculate the phonon self-energy, we need to know the momentum dependence of the electron–phonon interaction $W_{k,q=0} = D_k\sqrt{\hbar/2M\omega_G}$, where D_k is the interband electron–phonon coupling strength, M is a carbon atom mass and ω_G is the optical phonon frequency. We find (see Supplementary Information) that in metallic tubes the electron–phonon coupling is momentum-independent for the LO mode, $D_k = D$, but it is negligibly small for the TO mode, such that $\Delta\omega_{TO} \approx 0$ in metallic tubes. In semiconducting tubes, D_k is finite and momentum-dependent for both LO and TO, such that $D^2_{k,LO} + D^2_{k,TO} = D^2$ and $D^2_{k,LO} = D^2\alpha((\varepsilon_k - \Delta)/\Delta)(\beta + ((\varepsilon_k - \Delta)/\Delta))^{-1}$, and we use $\alpha \approx 1.1$ and $\beta \approx 0.4$ (see Supplementary Information). We use equations (1) and (2) to calculate the Raman shift and the width in both metallic nanotubes and graphene using the linear dispersion $\varepsilon_k = \pm\hbar v_F|k|$, and semiconducting nanotubes using the hyperbolic carrier dispersion $\varepsilon_k = \pm\sqrt{\Delta^2 + \hbar^2 v_F k^2}$, where $v_F = 10^6\ \mathrm{m\,s^{-1}}$ is the graphene Fermi velocity and Δ is half the bandgap. An optical bandgap of $2\Delta_{op} \approx 0.9\,d^{-1}$ eV nm (d is the tube diameter) has been corrected by the exciton binding energy of $E_b \approx 0.34\,d^{-1}$ eV nm (ref. 39) to give $2\Delta = 2\Delta_{op} + E_b$. The results for the Raman shifts are evaluated at zero temperature in leading order of charge density (or Fermi level ε_F) for graphene, LO mode in metallic, and both LO and TO modes in semiconducting nanotubes, respectively:

$$\Delta\hbar\omega_{\mathrm{Graphene}} = \lambda\left(\frac{\varepsilon_F}{\hbar\omega_G} + \frac{1}{4}\ln\left(\frac{2\varepsilon_F - \hbar\omega_G}{2\varepsilon_F + \hbar\omega_G}\right)\right) \approx \lambda\sqrt{\frac{\rho_C}{\rho_0}} \qquad (3a)$$

$$\Delta\hbar\omega_{\mathrm{Metallic,LO}} = \lambda\frac{d_0}{2d}\ln\left|\left(\frac{2\varepsilon_F}{\hbar\omega_G}\right)^2 - 1\right| = \lambda\frac{d_0}{2d}\ln\left|\left(\frac{d\rho_C}{d_0\rho_0}\right)^2 - 1\right| \qquad (3b)$$

$$\Delta\hbar\omega_{\mathrm{Semicond,LO}} + \Delta\hbar\omega_{\mathrm{Semicond,TO}} = \lambda\frac{d_0}{d}\left(\ln\left(\frac{\varepsilon_F + \sqrt{\varepsilon_F^2 - \Delta^2}}{\Delta}\right) + \frac{b}{\sqrt{1-b^2}}\,\mathrm{atan}\left(\frac{b}{\sqrt{1-b^2}}\frac{\sqrt{\varepsilon_F^2 - \Delta^2}}{\varepsilon_F}\right)\right) \approx \lambda\frac{\rho_C}{\rho_0}\frac{b}{1-b^2} \qquad (3c)$$

and

$$\Delta\hbar\omega_{\mathrm{Semicond,LO}} \approx \lambda\frac{\alpha}{6}\left(\frac{\rho_C}{\rho_0}\right)^3\left(\frac{d}{d_0}\right)^2\frac{b^3}{1-b^2} \qquad (3d)$$

where the electron–phonon coupling constant λ is given by $\lambda = AD^2/\pi M v_F^2$, with both spin and valley degeneracies included.

© 2007 Nature Publishing Group

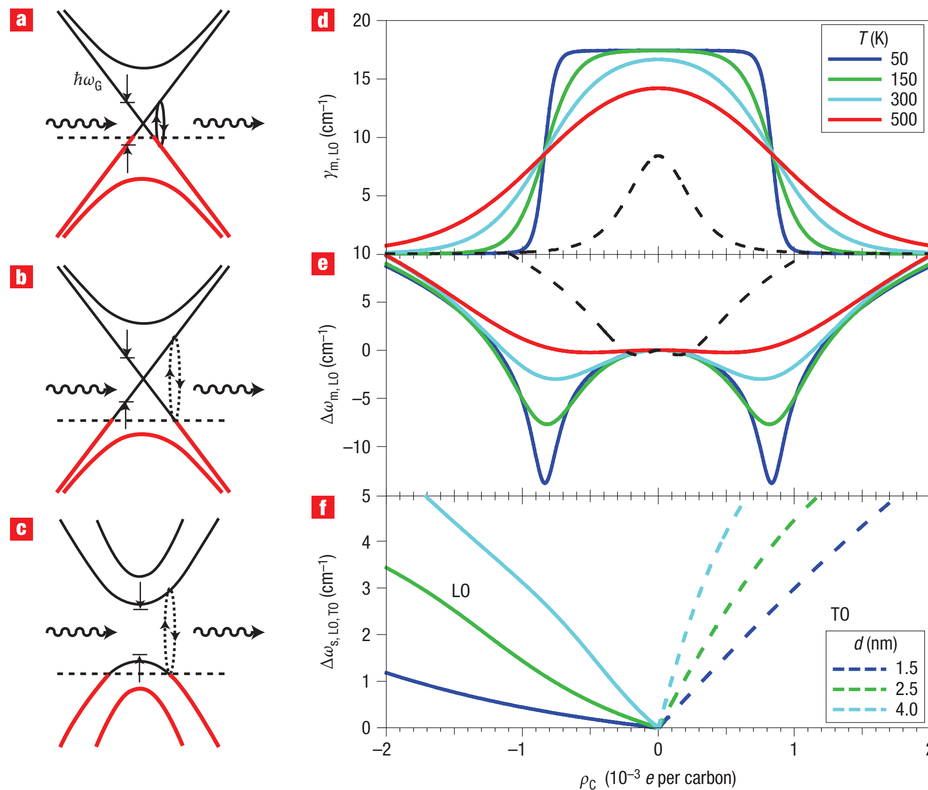

Figure 3 Frequency renormalization and broadening of the CNT G-phonon mode by the electron–phonon interaction. a–c, Scattering mechanisms for a metallic tube where the G mode can excite electron–hole pairs (**a**), a doped metallic tube where the phonon can only excite virtual electron–hole pairs (**b**) and a semiconducting tube where the bandgap is larger than the phonon energy, and no real electron–hole pairs can be created by the phonon (**c**). **d–f**, Calculations of the Raman width in a metallic tube ($d = 2.0$ nm) as a function of the charge carrier density per carbon atom at different T (**d**), corresponding G-mode Raman shifts (**e**) and Raman shift of the LO mode (solid lines) and TO modes (dashed lines) in semiconducting tubes at temperatures $T = 300$ K for different tube diameters, d, as a function of carrier density, $D = 10$ eV Å^{-1} (**f**). Black dashed lines in **d** and **e** are Raman width and shift, respectively, of graphene at 300 K.

Here, $b = \hbar\omega_G/2\Delta$ is a dimensionless phonon energy, $A \approx 5.24$ Å^2 is the area of the graphene unit cell, $d_0 = 2v_F/\pi\omega_G \approx 2$ nm is a characteristic length scale and $\rho_0 = eA\omega_G^2/2\pi v_F^2 \approx 0.00085e/\text{carbon}$ is the characteristic induced charge on a carbon atom. Note that a linear charge density in a CNT of diameter d is related to the induced charge on a carbon atom ρ_C by $\rho = 2\rho_C\pi d/A$. The functional dependences on charge carrier density are different in semiconducting and metallic CNTs, and in graphene, because of differences in the density of states. These differences and their consequences are depicted in Fig. 3 for (a) a metallic tube where the G mode can excite electron–hole pairs, giving rise to the broadening of the Raman signal, (b) a doped metallic tube where the phonon can only excite virtual electron–hole pairs, leading to an energy renormalization but no broadening, and (c) a semiconducting tube where the bandgap is larger than the phonon energy, and no real electron–hole pairs can be created by the phonon so that the energy is renormalized but the linewidth unchanged.

To simulate the experimental results using equation (2) one needs to know the electron–phonon coupling constant D, the Fermi velocity and the tube diameter d, which enables the bandgap Δ of the semiconducting tubes to be determined. The tube diameter is determined by measuring the ring breathing mode frequency, and the Fermi velocity is taken to be that of graphene. We are therefore left with just one unknown parameter: the electron–phonon coupling D. To obtain doping densities, one also needs to know the gate capacitance C and the threshold voltage V_{th}. When an operating FET device is studied, V_{th} can be determined from the electrical measurements (at the breakpoint in the I_d versus V_g curve). We stress that, in the present study, we are looking for the gate-induced changes on the phonon frequency and lifetime. If one wants to compare the absolute phonon frequency with the theoretical simulation one needs to offset the simulated frequency by the frequency of the undoped tube ω_G, which can be viewed here as a fit parameter. However, the Raman frequencies of the pristine (undoped) metallic and semiconducting tubes are functions of the tube diameter and can, in principle, like the excitation energies, be tabulated.

In addition to the difference in the density of states, different momentum dependencies of the interband electron–phonon matrix element for LO and TO modes in semiconducting tubes lead to different carrier concentration dependencies of the phonon shifts $\Delta\omega_{TO} \propto \rho$ and $\Delta\omega_{LO} \propto \rho^3$ at low temperatures. At room temperature, electron–hole pair excitation can take place away from the bottom of the bands, which makes the LO shift grow nearly linear with density, but with a much smaller slope than the TO mode shift. However, the overall size of the effect is determined by the same electron–phonon coupling constant λ. The maximum width of the optical phonon (Raman width) in graphene is given by the strength of the electron–phonon interaction as $\gamma_G = \pi\lambda/4$, and it also depends on the tube diameter as $\gamma_{M,LO} = \pi\lambda d_0/(2d)$ in metallic CNTs. From the

© 2007 Nature Publishing Group

maximum Raman width in graphene[14,15] of $8.5\,cm^{-1}$, an interband transition electron–phonon coupling $\lambda \approx 11\,cm^{-1}$ or $D \approx 10\,eV\,Å^{-1}$ has been extracted. In a metallic tube with $d = 2.35\,nm$ (see Supplementary Information) the Raman linewidth is $22\,cm^{-1}$, implying an interband electron–phonon coupling of $\lambda \approx 17\,cm^{-1}$, or $D \approx 13\,eV\,Å^{-1}$.

The numerical results for calculated Raman shifts and FWHMs, according to equation (1) and (2), are shown in Fig. 3d–f for metallic and semiconducting CNTs, respectively. The results are plotted against ρ_C, which is related linearly by electrostatics to the applied gate voltage. In metallic tubes, both LO phonon lifetime and energy are predicted to show strong temperature dependence, whereas in semiconducting tubes the TO mode shifts are predicted to be nearly temperature independent and the LO mode is temperature dependent for small doping levels. In semiconducting tubes, the TO mode phonon shift is approximately linearly proportional to both diameter and induced charge on the carbon atom, as shown by the red dotted line in Fig. 2c. If the phonon shift is plotted versus linear density ρ, it is predicted to be nearly independent of tube diameter in semiconducting tubes for the TO mode and inversely proportional to the tube diameter in metallic tubes for the LO mode. Note that the theoretical treatment of metallic tubes has also been considered recently in ref. 36.

The agreements between the magnitudes of the experimentally measured and theoretically derived shifts in the phonon energies for both semiconducting and metallic CNTs are quite reasonable, as is the agreement between experiment and theory for the gate-voltage-induced changes of the metallic CNT phonon linewidth for our ~2.4-nm-diameter CNTs. Deviations in the shape of the functional dependences of the phonon frequency shifts on V_g arise from trapped charges in the oxide substrate, which are not included in the calculation. These results also show that the virtual transitions in the semiconducting CNT are quite effective in renormalizing the optical phonon energy. In fact, when the bandgap of the semiconducting CNT is in resonance with the Raman phonon energy, as is the case for a ~5-nm CNT, the renormalization of the phonon energy can be larger than that observed for the graphene device. This reflects the high density of electronic states at the bandgap in the semiconducting 1D CNTs.

As we saw in metallic CNTs, a V_g-induced shift in the Fermi level (charge density) leads to blueshifts of $\sim 10\,cm^{-1}$ and a broadening of $\sim 15\,cm^{-1}$ for the G phonon of metallic nanotubes. This situation is totally analogous to those recently reported from Raman scattering experiments on graphene FETs (refs 14, 15). For graphene on a 300-nm oxide, application of $V_g = 100\,V$ produced a $10\,cm^{-1}$ shift to higher energies of the G line and a $10\,cm^{-1}$ reduction in the phonon linewidth. Similar behaviour is expected, because the band structure in the vicinity of the Fermi level of a metallic CNT is similar to that of graphene. The observation that a sharp G line in a metallic CNT after the Fermi level was moved into the valence band is interesting in light of the long-standing discussion of the mechanism by which the G^- line in metallic CNTs is broadened[40].

In semiconducting nanotubes, however, we also observed a similar shift in the phonon energy, but no change in linewidth. As the sample is now a semiconductor, we do not have the Fermi surface required to produce the gate-voltage-dependent damping invoked by others to explain their graphene results[14,15]. For our 2.4-nm CNT, we expect a $\sim 5\,cm^{-1}$ shift, close to what we observe in the conducting state. However, we do predict a different temperature dependence of the Raman shift as a function of charge density in metallic and semiconducting CNTs. The renormalization becomes smaller as the tube diameter decreases, because of the increasing size of the bandgap. As the tube diameter increases, the phonon renormalization increases and peaks at a diameter where the bandgap is equal to the phonon energy.

Carbon nanotubes and graphene are closely related materials. The anomalous dependence of the graphene G-line energies on gate voltage has been attributed to the unique character of its low-lying electronic states. Surprisingly, however, we find similar behaviour on the part of the G phonon in a 2.4-nm-diameter semiconducting CNTFET as a function of gate voltage. We explain these shifts in the phonon energy as a function of gate voltage due to the renormalization of the LO phonon energy by the gate-induced carriers in the 1D semiconducting CNT. As such, it suggests that the energy of the G mode in semiconducting CNTFETs provides a new way to monitor the local Fermi level in a semiconducting CNTFET. Our optical probe can have dimensions as small as 250 nm, allowing us to observe changes in the Fermi level near contacts, defects and trapped charges, or resulting from charge transfer effects. It also provides an additional means of understanding the large variation in the observed G-line energies of CNTs on SiO_2 substrates, and the failure to observe G-line energies converging to the graphite/graphene limit in large-diameter CNTs (refs 24, 41).

Note added in proof: After this manuscript was submitted, a paper was published on the subject of gate-induced broadening of the G mode of metallic nanotubes[42].

Received 11 May 2007; accepted 24 August 2007; published 14 October 2007.

References

1. *International Technology Roadmap for Semiconductors: 2005 Edition* (Semiconductor Industry Association, 2005). Available online at http://www.itrs.net/Links/2005ITRS/Home2005.htm, 2005.
2. Avouris, P. Carbon nanotube electronics. *Proc. IEEE* **91,** 1772–1784 (2003).
3. Avouris, P. Electronics with carbon nanotubes. *Phys. World* **20,** 40–45 (March 2007).
4. McEuen, P. L., Fuhrer, M. & Park, H. Single-walled carbon nanotube electronics. *IEEE Trans. Nanotechnol.* **1,** 78–85 (2002).
5. Javey, A. *et al.* Carbon nanotube field-effect transistors with integrated ohmic contacts and high-*k* gate dielectrics. *Nano Lett.* **4,** 447–450 (2004).
6. Chen, J. *et al.* Self-aligned carbon nanotube transistors with charge transfer doping. *Appl. Phys. Lett.* **86,** 123108 (2005).
7. Klinke, C. *et al.* Charge transfer induced polarity switching in carbon nanotube transistors. *Nano Lett.* **5,** 555–558 (2005).
8. Fan, Y., Goldsmith, B. R. & Collins, P. G. Identifying and counting point defects in carbon nanotubes. *Nat. Mater.* **4,** 906–911 (2005).
9. Mannik, J. *et al.* Chemically induced conductance switching in carbon nanotube circuits. *Phys. Rev. Lett.* **97,** 016601 (2006).
10. Fuhrer, M. S. *et al.* High-mobility nanotube transistor memory. *Nano Lett.* **2,** 755–759 (2002).
11. Kim, W. *et al.* Hysteresis caused by water molecules in carbon nanotube field-effect transistors. *Nano Lett.* **3,** 193–198 (2003).
12. Freitag, M. *et al.* Electrically excited, localized infrared emission from single carbon nanotubes. *Nano Lett.* **6,** 1425–1433 (2006).
13. Strano, M. S. *et al.* Reversible, band-gap-selective protonation of single-walled carbon nanotubes in solution. *J. Phys. Chem. B* **107,** 6979–6985 (2003).
14. Pisana, S. *et al.* Breakdown of the adiabatic Born–Oppenheimer approximation in graphene. *Nat. Mater.* **6,** 198–201(2007).
15. Yan, J. *et al.* Electric field effect tuning of electron–phonon coupling in graphene. *Phys. Rev. Lett.* **98,** 166802 (2007).
16. Dresselhaus, M. S. & Dresselhaus, G. Intercalation compounds of graphite. *Adv. Phys.* **30,** 139–326 (1981).
17. Su, W. P., Schrieffer, J. R. & Heeger, A. J. Solitons in polyacetylene. *Phys. Rev. Lett.* **42,** 1698–1701 (1979).
18. Su, W. P., Schrieffer, J. R. & Heeger, A. J. Soliton excitations in polyacetylene. *Phys. Rev.* **22,** 2099–2111 (1980).
19. Perebeinos, V., Tersoff, J. & Avouris, P. Effect of exciton-phonon coupling in the calculated optical absorption of carbon nanotubes. *Phys. Rev. Lett.* **94,** 027402 (2005).
20. Kuper, C. G. & Whitfield, G. D. *Polarons and Excitons* (Plenum Press, New York, 1963).
21. Piscanec, S. *et al.* Kohn anomalies and electron–phonon interactions in graphite. *Phys. Rev. Lett.* **93,** 185503 (2004).
22. Peierls, R. E. *Quantum Theory of Solids* (Clarendon Press, Oxford, 1955).
23. Wilson, J. A., Di Salvo, F. J. & Mahajan, S. Charge-density waves and superlattices in the metallic layered transition metal dichalcogenides. *Adv. Phys.* **24,** 117–201 (1975).
24. Piscanec, S. *et al.* Optical phonons in carbon nanotubes: Kohn anomalies, Peierls distortions, and dynamic effects. *Phys. Rev. B* **75,** 035427 (2007).
25. Yao, Z., Kane, C. L. & Dekker, C. High-field electrical transport in single-wall carbon nanotubes. *Phys. Rev. Lett.* **84,** 2941–2944 (2000).
26. Javey, A. *et al.* High-field quasiballistic transport in short carbon nanotubes. *Phys. Rev. Lett.* **92,** 106804 (2004).
27. Park, J. Y. *et al.* Electron–phonon scattering in metallic single-walled carbon nanotubes. *Nano Lett.* **4,** 517–520 (2004).

© 2007 Nature Publishing Group

28. Perebeinos, V., Tersoff, J. & Avouris, P. Electron–phonon interaction and transport in semiconducting carbon nanotubes. *Phys. Rev. Lett.* **94,** 086802 (2005).
29. Lazzeri, M. *et al*. Phonon linewidths and electron–phonon coupling in graphite and nanotubes. *Phys. Rev. B* **73,** 155426 (2006).
30. Dresselhaus, M. S. *et al*. Raman spectroscopy of carbon nanotubes. *Phys. Rep.* **409,** 47–99 (2005).
31. Allen, P. B. Neutron spectroscopy of superconductors. *Phys. Rev. B* **6,** 2577–2579 (1972).
32. Allen, P. B. & Silberglitt, R. Some effects of phonon dynamics on electron lifetime, mass renormalization, and superconducting transition temperature. *Phys. Rev. B* **9,** 4733–4741 (1974).
33. Lazzeri, M. & Mauri, F. Nonadiabatic Kohn anomaly in a doped graphene monolayer. *Phys. Rev. Lett.* **97,** 266407 (2006).
34. Ando, T. Anomaly of optical phonon in monolayer graphene. *J. Phys. Soc. Jpn* **75,** 124701 (2006).
35. Neto, A. C. & Guinea, F. Electron–phonon coupling and Raman spectroscopy in graphene. *Phys. Rev. B* **75,** 045404 (2007).
36. Caudal, N. *et al*. Kohn anomalies and nonadiabaticity in doped carbon nanotubes. *Phys. Rev. B* **75,** 115423 (2007).
37. Popov, V. N. & Lambin, P. Resonant Raman intensity of the totally symmetric phonons of single-walled carbon nanotubes. *Phys. Rev. B* **73,** 165425 (2006).
38. Jiang, J. *et al*. Exciton–photon, exciton–phonon matrix elements, and resonant Raman intensity of single-wall carbon nanotubes. *Phys. Rev. B* **75,** 035405 (2007).
39. Dukovic, G. *et al*. Structural dependence of excitonic optical transitions and band-gap energies in carbon nanotubes. *Nano Lett.* **5,** 2314–2318 (2005).
40. Paillet, M. *et al*. Vanishing of the Breit–Wigner–Fano component in individual single-wall carbon nanotubes. *Phys. Rev. Lett.* **94,** 237401 (2005).
41. Gupta, A. *et al*. Raman scattering from high-frequency phonons in supported n-graphene layer films. *Nano Lett.* **6,** 2667–2673 (2006).
42. Wu, Y. *et al*. Variable electron–phonon coupling in isolated metallic carbon nanotubes observed by Raman scattering. *Phys. Rev. Lett.* **99,** 027402 (2007).

Acknowledgements

Correspondence and requests for materials should be addressed to P.A.
Supplementary information accompanies this paper on www.nature.com/naturenanotchnology.

Reprints and permission information is available online at http://npg.nature.com/reprintsandpermissions/

© 2007 Nature Publishing Group